Vol. 29 (1998) *ACTA PHYSICA POLONICA B* No 8

FRAGMENTATION OF THE Pb PROJECTILE AT 158 GeV/NUCLEON IN Pb–Pb INTERACTIONS

M.L. Cherry[b], A. Dąbrowska[a], P. Deines-Jones[b †], R. Hołyński[a]
B.S. Nilsen[b ‡], A. Olszewski[a], M. Szarska[a], A. Trzupek[a]
C.J. Waddington[c], J.P. Wefel[b], B. Wilczyńska[a], H. Wilczyński[a]
W. Wolter[a], B. Wosiek[a] and K. Woźniak[a]

For the KLM Collaboration

[a] Institute of Nuclear Physics, Kawiory 26A, 30-055 Kraków, Poland
[b] Louisiana State University, Baton Rouge, LA 70803, USA
[c] University of Minnesota, Minneapolis, MN 55455, USA

(Received June 2, 1998)

We have investigated the process of fragmentation of the Pb nucleus at 158 GeV/nucleon in Pb–Pb interactions recorded in lead-emulsion chambers of the EMU13 CERN experiment. The number of Pb–Pb interactions found was larger than that expected from the nuclear charge changing cross section which indicates an important role of electromagnetic dissociation processes in Pb–Pb interactions at this high energy. The emission angles of multiply charged projectile fragments as well as of spectator protons were measured using the semiautomated device with the CCD camera mounted on a microscope. Taking the advantage of the unconventional design of the emulsion chambers the charges of all multiply charged projectile fragments were measured. On the basis of these measurements, different modes of the Pb projectile break-up are discussed. The rates and properties of the fragmentation processes such as fission, multifragmentation and disintegration only into singly charged fragments are presented.

PACS numbers: 25.75. +r, 29.40. Rg

1. Introduction

The main interest in studying interactions of relativistic heavy nuclei at ever higher energies is the possibility of creating the nuclear matter of high density and temperature and subsequent investigation of the properties of

† Present address: NASA Goddard Space Flight Center, Greenbelt, MD 20771, USA.
‡ Present address: Ohio State University, Columbus, OH 43210, USA.

nuclear matter under such extreme conditions. These studies are mostly focused on the first stage of the collision process, when nucleons from the two colliding nuclei interact via a strong force and produce secondary particles. During this production process some fraction of the available energy is transferred to the spectator parts of colliding nuclei, leaving those nuclear remnants in an excited state. On a longer time scale, the de-excitation of the nuclear remnants takes place. It is the latter process called nuclear fragmentation, and in particular the fragmentation of the relativistic projectile nucleus in which we are interested here. The fragmentation of a heavy projectile leads to the emission of fragments with a broad mass spectrum which extends from the lightest fragments, *i.e.* nucleons, to the fragments as heavy as the disintegrating projectile. This broad mass range is correlated with the large range of fragment multiplicities. Thus, we observe a large diversity of fragmentation modes which may correspond to different break-up mechanisms: from emission of a single heavy fragment, through binary fission to a complete break-up into nucleons.

The fragmentation of light projectile ions, oxygen and sulphur, at the energy of 200 GeV/nucleon have been investigated in conventional emulsion stacks experiments [1, 2]. The same technique was used to study the fragmentation of gold projectile accelerated to an energy of 10.6 GeV/nucleon at AGS [3–8]. Experiments with the emulsion stacks, irradiated by ion beams parallel to the emulsion surface, are suitable for studying the process of the projectile fragmentation thanks to the possibility of charge measurements for all forward emitted fragments. The studies of the gold fragmentation at energies up to 10.6 GeV/nucleon showed that the fragmentation of the heavy projectile depends on the mass of the target nucleus [5, 7] and a more violent break-up of the projectile was observed for heavier target nuclei. It was also shown that below the energy of 10.6 GeV/nucleon the hypothesis of a limiting fragmentation is not valid [3, 4].

The acceleration of Pb ions to an energy of 158 GeV/nucleon opens the possibility of investigating the fragmentation of a heavy projectile at energy more than an order of magnitude higher. However, at such high energy the fragmentation process cannot be any longer efficiently studied with the use of the emulsion stack method. This drawback is due to the fact that at high energies projectile fragments are strongly collimated in the forward cone. Therefore their charges and emission angles can be measured only at a large distance from the interaction vertex. But, in this case, the probability of secondary interactions of heavy projectile fragments in the dense emulsion environment is high. In effect, heavy fragments often undergo secondary interaction before being resolved and available for charge and angular measurements. In contrast to the emulsion stacks, emulsion chambers, composed of nuclear target foils and thin emulsion plates interleaved with spacers, al-

low for precise measurements of forward going fragments. The amount of matter traversed by fragments throughout the chamber is small, reducing significantly the probability of secondary interactions and making possible angular measurements at large distances from the interaction point. In addition, a unique construction of the emulsion chambers used in the EMU13 experiment enables charge measurements of all projectile fragments with an accuracy sufficient to study different fragment topologies.

In this paper we present the results on the fragmentation of the Pb projectile after an interaction with lead target at 158 GeV/nucleon, obtained in the CERN EMU13 experiment performed by Kraków–Louisiana–Minnesota Collaboration. The paper is organized as follows: In Section 2 the structure of the EMU13 chamber is described and details on scanning and measurements are given. Section 3 contains a discussion of the measured cross section for Pb–Pb interactions. In Section 4 characteristics of the fragmentation of the Pb projectile are presented and some fragmentation channels are discussed. Finally, Section 5 includes a summary and concluding remarks.

2. Experiment

2.1. Emulsion chambers

Emulsion chambers with lead targets were exposed to the 158 GeV/nucleon Pb beam from the SPS accelerator at CERN. The chambers were irradiated perpendicularly to the lead-emulsion layers by Pb ions with densities ranging from 500 to 1000 particles/cm^2. The same emulsion chambers were used to study particle production in central Pb–Pb collisions [9].

Each chamber was composed of three modules. A schematic drawing of the chamber is depicted in Fig. 1. The target module (T) consisted of three or four lead foils, 100 μm thick, and with the surface dimensions of 5×10 cm^2 interleaved by two emulsion plates. One emulsion plate was placed at the top of the chamber. The 5×10 cm^2 plates were double coated by 55 μm thick Fuji ET7B emulsion on a 200 μm acrylic base. The same kind of emulsion plates were used in the angular measurement module (M) which followed the target section. The angular measurement module consisted of several spacers of gradually increasing thicknesses interleaved by emulsion plates, spaced out approximately 17 cm from the last Pb target foil to the final emulsion plate. Altogether there were 20 emulsion plates in the target and angular measurement modules. The last module (C), at the bottom of the chamber, was designed for charge measurements of projectile fragments. It was composed of three emulsion pellicles, 500 μm thick, of the dimensions 10×10 cm^2 placed one after another at the angle of about 20° with respect to the beam direction. This ensured that the total length of a multiply charged

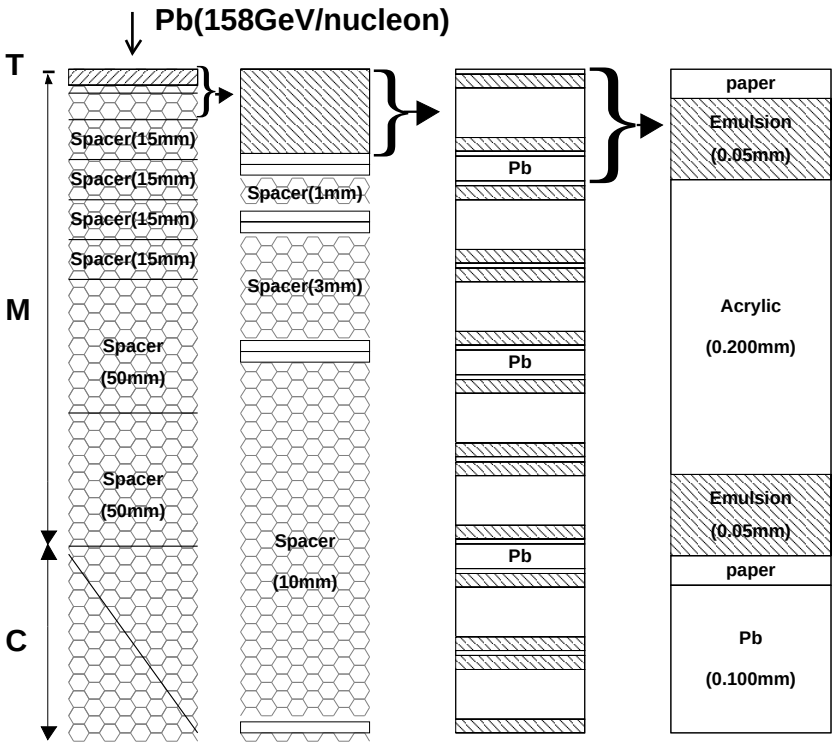

Fig. 1. EMU13 emulsion chamber: the left most drawing displays the layout of the whole chamber; other drawings show blown up parts of the chamber.

fragment was about 4.5 mm in these three emulsion pellicles. This length was sufficient to perform δ-ray counts on the basis of which the charges of Pb projectile fragments were estimated. A link established between these three modules allowed an event to be followed from one module to the other.

2.2. Scanning for Pb–Pb interactions

The scanning for minimum bias Pb–Pb interactions was performed by a simultaneous inspection of the top and the bottom plate from the target module, under the microscope using magnification of 225×. The initial selection consisted of events for which a noticeably smaller size of the spot was observed at the bottom plate as compared to the corresponding spot of the entering Pb track at the top emulsion layer and events which showed a developed shower of secondary particles at the bottom plate. Each selected event was then followed upstream, starting from the bottom target plate, in order to localize the interaction vertex. Doubtful positions of interaction vertices were further checked by measuring the convergence of secondary

tracks emitted at large angles. Out of 64112 Pb tracks entering the top plate of the target, 2494 Pb tracks interacted in the target module and out of these 566 in Pb foils.

Our scanning was inefficient in finding events characterized by low multiplicities of singly charged relativistic particles accompanied by a single heavy projectile fragment with the charge not very different from that of the primary. In consequence we have missed some very peripheral interactions with no apparent charge change (approximately of the five charge units or less). The emulsion measurements of the fragmentation of the gold nucleus at 10.6 GeV/nucleon suggest [10] that some 5–10% of interactions have such small charge changes. On the basis of the extrapolation of the parameterization of the partial charge changing cross sections measured at low energies [11] to the Pb–Pb collisions at 158 GeV/nucleon we estimated that the interactions with the charge change up to five charge units should constitute about 10% of the nuclear charge changing cross section. This bias should not affect the investigation of the fragmentation channels characterized by an emission of more than one fragment, like fission or multifragmentation processes. On the other hand, this inefficiency leads a systematic uncertainty (less than 10%) in the rates for different processes. Interestingly, despite this scanning bias, the number of Pb–Pb interactions found was significantly larger than that expected from the nuclear charge changing cross section. This discrepancy can be explained by a contribution of the electromagnetic dissociation (ED) processes which play an important role in interactions of heavy ions at high energies. The ED processes will be discussed in one of the following Sections.

2.3. Measurements

Out of 566 Pb–Pb interactions found, we have analyzed 454 events, leaving out the events accompanied with nearby noninteracting Pb primaries which might obscure the measurements as well as the events for which a secondary interaction on the unresolved core of tracks was recorded in the closest vicinity to the primary vertex.

For each analyzed event, the angular measurements of shower particles and multiply charged projectile fragments were performed in the angular measurement module within the restricted angular region $\theta \leq 5$ mrad corresponding to pseudorapidity $\eta = -\ln\tan(\theta/2) \geq 6$. The measurements were performed using the system which digitizes the emulsion images (a CCD camera mounted on a microscope and coupled to the PC) and allows for automatic track coordinate measurements with sub-micron precision.

The charge measurements of multiply charged projectile fragments were carried out in the bottom module of the chamber. The δ-ray counts were

taken in the three thick emulsion pellicles on the track length of about 3mm. Thus the number of the δ-rays counted per fragment was limited by geometry. Consequently, the uncertainties in charge determination were of the order of 10 % for charges above 30 and of the order of 1–2 charge units for lighter fragments.

The angular measurements were made over the distance of about 20 cm, with the precision of about 0.2μm for track measurements in the transverse plane. Therefore, the uncertainty of the track opening angles is mainly due to the uncertainty in the position of the event axis, *i.e.*, the direction of the primary Pb nucleus. The axis position was determined as the coordinate center weighed by particle mass and calculated for all multiply charged fragments and singly charged particles forming a most densely populated region. Thus the angular measurement uncertainty of a particular track strongly depends on the fragmentation mode, being the smallest for events with one heavy fragment or for multifragmentation events. The overall uncertainty in the pseudorapidity was estimated to be less than 0.02 η units.

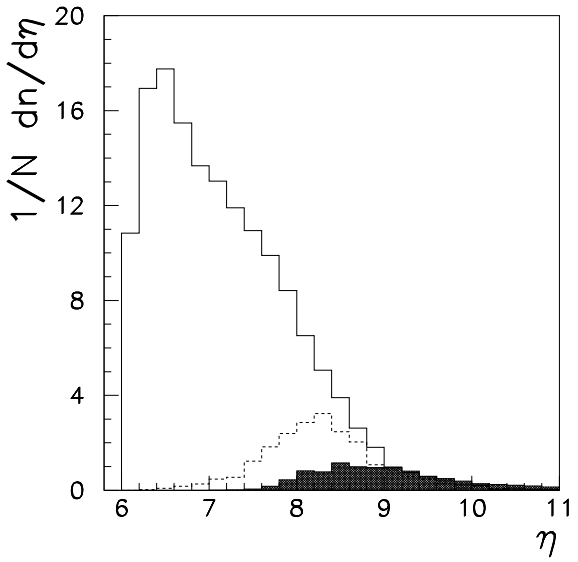

Fig. 2. Pseudorapidity distributions of singly charged particles — solid line, helium fragments — dashed line and heavier ($Z \geq 3$) fragments — shaded histogram.

The pseudorapidity distributions of singly charged relativistic particles, helium fragments and particles heavier than helium are shown in Fig. 2. For η values greater than about 6.2 ($\theta \leq 4$ mrad) the distribution of singly charged particles is practically unbiased. From our previous analysis of oxygen and sulphur interactions at 200 GeV/nucleon [1] it followed that within a 3 mrad half opening cone ($\eta \geq 6.5$) almost all spectators are contained and the number of produced particles is small. This was confirmed using the VENUS Monte Carlo Model [12]. Shifting the η value of 6.5 by ln(158/200) we define the fragmentation region of the Pb(158 GeV/nucleon) projectile as that with $\eta \geq 6.26$. Thus, we can conclude from Fig. 2 that the range of our unbiased angular measurements covers the region of the Pb projectile fragmentation.

3. Pb–Pb cross section

The experimentally measured total cross section for the detected Pb–Pb interactions is: $\sigma_{\mathrm{tot}}^{\mathrm{exp}} = 8.7$ b. This cross section was calculated using the measured initial flux of Pb nuclei, Pb target thicknesses and the number of 566 found events. The charge changing cross section for nucleus–nucleus collisions due to the strong interaction, σ_{nucl}, calculated from the parameterization of cross sections measured at low energies [11], equals 6.9 b with the uncertainty of the order of 10 %. Clearly, the measured cross section exceeds σ_{nucl}. Thus, we observe an excess of events (corresponding to about 1.8 b) which can be attributed to electromagnetic processes. It is predicted [13] that for heavy ion collisions the processes of electromagnetic dissociation (ED) become important. Furthermore, the cross section for ED, σ_{ED}, increases approximately logarithmically with the energy, and for high energy and heavy colliding nuclei it exceeds the cross section for nuclear interactions. The ED is expected to play an important role in the process of nuclear fragmentation.

Electromagnetic dissociation can occur when a projectile nucleus passes near a heavy target with an impact parameter, b, beyond the range of nuclear force, whereas strong interaction processes dominate when nuclei penetrate each other. A projectile nucleus in distant collision with a target nucleus (without any nuclear contact), is excited by strong electromagnetic fields of short duration. The electromagnetic pulse provided by a target nucleus can be sufficiently energetic to excite giant resonances in the projectile, or to create particles (e^+e^- pairs, pions, heavy leptons *etc.*). The description of the ED mechanism in relativistic heavy ion collisions is based on the equivalent photon method developed by Weizsäcker and Williams (W–W) [14]. The electromagnetic pulse seen by the projectile is equivalent to a number of virtual photons per unit area of the projectile. Using the

W–W method, the number of virtual photons of energy E_γ per unit area and energy interval is :

$$N_\gamma(E_\gamma) = \frac{2}{\pi}\frac{Z_T^2}{\beta^2}\alpha\frac{1}{E_\gamma}\left\{xK_0(x)K_1(x) - 0.5\beta^2x^2\left[K_1^2(x) - K_0^2(x)\right]\right\}, \quad (1)$$

where K_i are modified Bessel Functions of order i, Z_T is the charge of the target nucleus, β is the velocity of the projectile in units of c, the fine structure constant. The variable $x = (E_\gamma b_{\min})/(\gamma\hbar c)$ is expressed in terms of the photon energy, the Lorentz factor of the projectile, γ, and depends on the minimal impact parameter, $b_{\min}$ above which all interactions are of electromagnetic nature. $b_{\min}$ is derived from the pure nuclear cross section: $b_{\min} = (\sigma_{\mathrm{nucl}}/\pi)^{1/2}$. The formula (1) is based on a classical treatment of the time dependent electromagnetic fields. In the case of a quantum mechanical approach [15] equivalent photon spectra are distinguished by multipolarities. However, it was shown [16] that classical W–W formula is a good approximation for high values of the Lorentz factor, $\gamma \gg 1$ (in our experiment $\gamma = 170$).

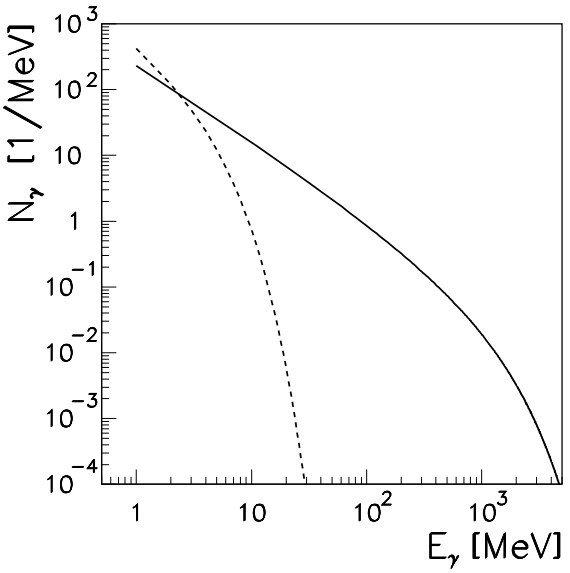

Fig. 3. Equivalent photon energy spectra seen by the Pb projectile at 158 GeV/nucleon (solid line) and 1 GeV/nucleon (dashed line) in Pb–Pb collisions.

The equivalent photon spectrum calculated for Pb–Pb collisions at 158 GeV/nucleon is shown in Fig. 3. For comparison the $N_\gamma(E_\gamma)$ for the same

collision system, but for incident energy of 1 GeV/nucleon is also shown. One can see that the spectrum for high primary energy extends up to photon energies as high as few GeV. In order to calculate the total cross section for ED, the product of the equivalent photon spectrum and the appropriate photonuclear cross section, $\sigma_{\gamma A}(E_\gamma)$ should be integrated over the whole range of photon energies:

$$\sigma_{\mathrm{ED}}^{\mathrm{tot}} = \int_0^\infty N_\gamma(E_\gamma)\sigma_{\gamma A}(E_\gamma)dE_\gamma \,. \tag{2}$$

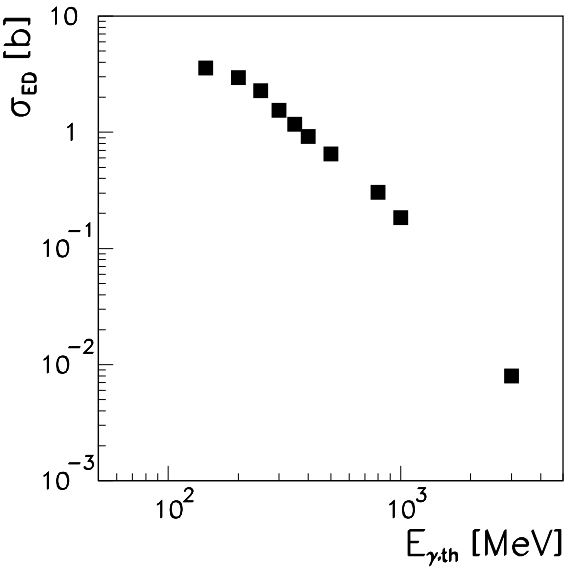

Fig. 4. Integrated photonuclear cross sections, $\sigma_{\mathrm{ED}}(E_\gamma \geq E_{\gamma,\mathrm{th}})$, as a function of the photon threshold energy, $E_{\gamma,\mathrm{th}}$ for Pb–Pb collisions at 158 GeV/nucleon.

To perform this integration one has to use experimentally measured $\sigma_{\gamma A}(E_\gamma)$. The estimate of $\sigma_{\mathrm{ED}}^{\mathrm{tot}}$ for Pb(158 GeV/nucleon)–Pb collisions is given in [17] and equals about 46 b. A similar value ($\sim$ 40 b) can be obtained by extrapolation of the experimentally measured $\sigma_{\mathrm{ED}}^{\mathrm{tot}}$ for different collision systems and at different energies [18]. In our experiment the majority of the events due to electromagnetic processes cannot be detected, since they lead to one-nucleon removal from the excited giant resonances, which occur for photon energies in the range of 10–30 MeV. For higher energies, $E_\gamma > 140$ MeV, photon interactions with a projectile nucleus are dominated by excitation of nucleon resonances which, due to their very short life-time, decay into nucleon and pion inside the nucleus. The two resulting energetic

hadrons may induce fragmentation of the nucleus by strong interaction. The latter phenomenon is then very similar to the interaction of a nucleon (or pion) with a nucleus. For very high photon energies ($E_\gamma > 2$–3 GeV), a photon has a non vanishing probability to transform into vector meson states, which strongly interact with a nucleus. Using experimentally measured photoproduction cross sections [19], we can estimate that the observed excess of events can be explained by electromagnetic interactions of photons with energies $E_\gamma > 280 \pm 20$ MeV(see Fig. 4), which represent about 4 % of the total ED cross section. Due to the arguments presented above the break-up of the Pb projectile induced by such high energy photons should not differ significantly from the break-up caused by nuclear interactions. In fact, in our data we do not see clear differences in the projectile fragmentation modes which would allow us to disentangle electromagnetic and nuclear processes. Therefore in the following Sections, we present the characteristics of a lead projectile fragmentation process for a sample of events consisting of about 80 % of nuclear and about 20 % of electromagnetic processes induced by high energy photons.

4. Fragmentation of the Pb projectile

4.1. General characteristics of the projectile break-up

The sample of the analyzed Pb–Pb interactions consists of 454 events. For each event analyzed we determined the number, N_s, of singly charged particles emitted within a forward cone ($\eta \geq 6.26$), the multiplicity, N_α, of alpha particles, and the number, N_f, of heavier($Z \geq 3$) fragments. The average numbers of the various types of particles emitted from the Pb projectile for the full sample of measured events are given in Table I. One can see that helium nuclei are the most frequent among the multiply charged fragments. The multiplicity distributions of alpha particles and heavier fragments are presented in Fig. 5. This figure shows that the range of the N_f-multiplicity distribution extends from 0 to 8 fragments and the distribution has a maximum at $N_f = 1$–2. The multiplicity distribution of alpha particles is much wider. It ranges from 0 to 14 with an approximately constant yield up to $N_\alpha \sim 7$. It is interesting to see the correlations between multiplicities of alpha particles and heavier fragments. One can see in Fig. 6 that the interactions in which several heavy fragments ($N_f \geq 3$) are emitted from the Pb projectile nucleus are also accompanied by several alpha particles. There is a considerable number of interactions in which the projectile breaks up into singly charged particles only, ($N_\alpha = N_f = 0$). These interactions represent 4.4 ± 1.0 % of all the analyzed events (5.6 % of $\sigma_{\rm nucl}$) and are mostly due to central collisions in which majority of the projectile nucleons have participated in the first stage of the collision, *i.e.*, in the process of particle production.

TABLE I

Mean numbers of singly charged particles, helium and heavier fragments for a full sample of Pb(158 GeV/nucleon)–Pb interactions, for fission events and multifragmentation processes. For each sample average charge of fragments heavier than helium, average charge bound in multiply charged fragments and average charge of the heaviest fragment are also listed.

	Full sample	Fission	Multifragmentation
$\langle N_s(\eta \geq 6.26)\rangle$	27.2 ± 0.6	1.44 ± 0.3	34.8 ± 0.9
$\langle N_\alpha \rangle$	4.26 ± 0.13	0.11 ± 0.07	5.8 ± 0.3
$\langle N_f \rangle$	2.03 ± 0.07	2.0	3.9 ± 0.1
$\langle Z_f \rangle$	16.12 ± 0.59	40.3 ± 0.1	6.3 ± 0.1
$\langle Z_b \rangle$	41.26 ± 1.16	80.8 ± 0.6	36.3 ± 1.3
$\langle Z_1 \rangle$	27.74 ± 1.06	43.8 ± 0.9	9.6 ± 0.4

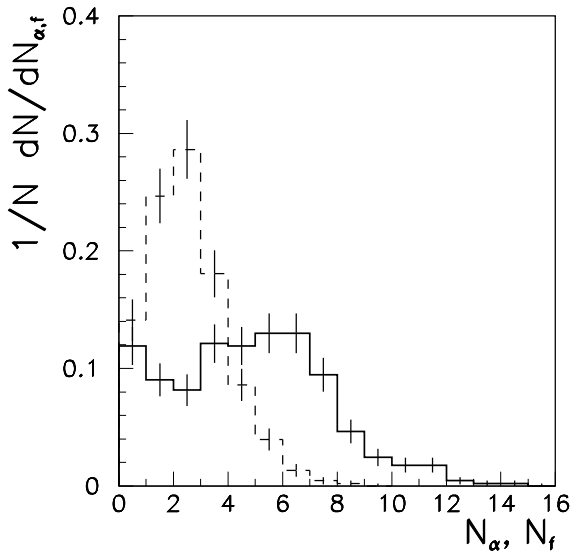

Fig. 5. Multiplicity distributions for helium (solid line) and heavier fragments (dashed line).

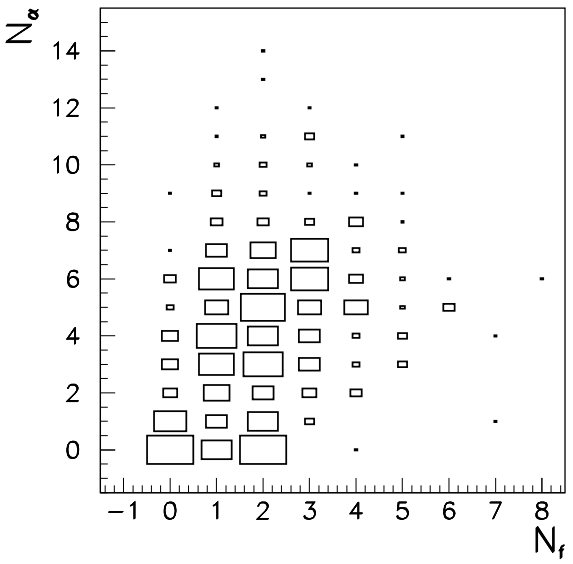

Fig. 6. Correlation between number of fragments, N_f, and number of alpha particles, N_α. The area of the box is proportional to the number of interactions with a given N_f and N_α.

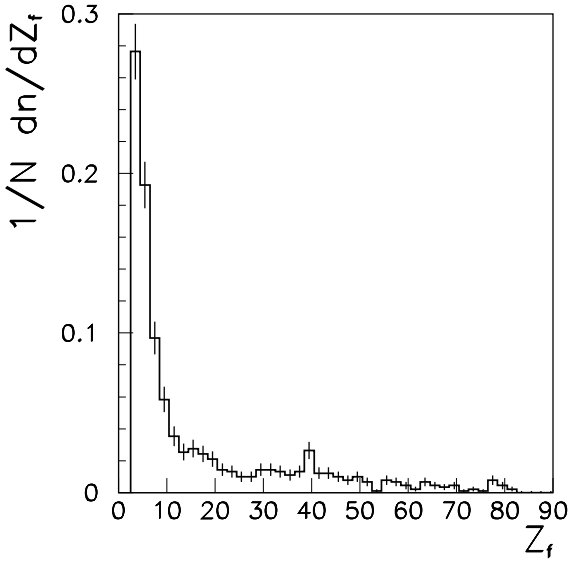

Fig. 7. Charge distribution of fragments with $Z \geq 3$.

The charge distribution of 922 fragments with $Z \geq 3$ is shown in Fig. 7. It is strongly peaked for light fragments, and shows an enhancement for the charge values $Z_f \approx 40$, which can be attributed to fission-like events (see the discussion below). The average charge of heavier fragments is relatively low (16.1 ± 0.6, see Table I) as compared to the projectile charge, $Z_p = 82$.

The total charge bound in multiply charged fragments, $Z_b = \sum_{i=1}^{N_f} Z_{f,i} + 2N_\alpha$ was also calculated. This quantity is proportional to the size of the projectile remnant. The Z_b distribution, shown in Fig. 8, is practically constant over the entire range of Z_b values. Consequently the average value of Z_b, listed in Table I, is close to the half of the projectile charge. The most frequent ED events, *i.e.* those with the one-nucleon removal, would produce a sharp peak at the Z_b values close to the projectile charge. Lack of such a structure confirms our earlier suggestions that the ED events which are included in the analyzed sample resemble, to a large extent, the events due to nuclear fragmentation. From the charge distribution of the heaviest

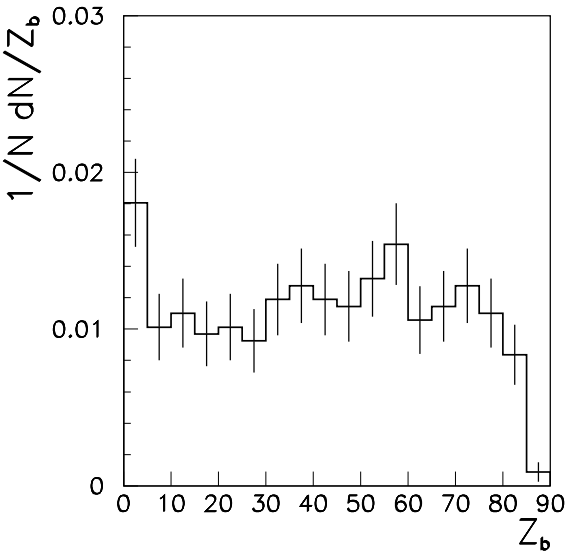

Fig. 8. Distribution of the charge bound in multiply charged fragments.

fragment in an event, Z_1, displayed in Fig. 9, it can be seen that in 77 % of interactions the heaviest fragment is lighter than half of the projectile charge. The average charge of the heaviest fragment is thus significantly smaller than half of the charge of the projectile nucleus (see Table I).

It was suggested [4] that the correlation between the heaviest (Z_1) fragment and the sum of the remaining charge bound in multiply charged fragments, $Z_r = Z_b - Z_1$ should be investigated. This correlation, displayed in Fig. 10, shows that there are many events where $Z_r > Z_1$. Furthermore, the

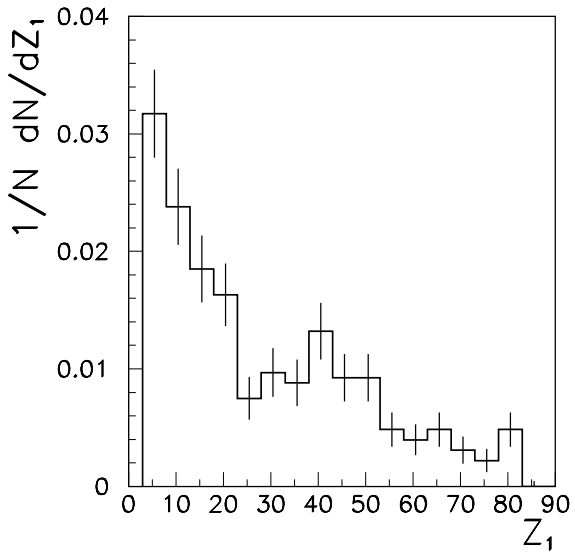

Fig. 9. Distribution of the charge of the heaviest fragment, Z_1, in an event.

events with a well defined leading fragment, *i.e.* $Z_1 > Z_p/2$, usually have a significant total charge bound in remaining fragments. The ratio R, defined as $R = Z_1/Z_r$ increases with increasing Z_b as it is shown in Fig. 11. It can also be seen that a well defined leading fragment ($R > 1$) can be found only in interactions characterized by a large Z_b, *i.e.* in peripheral collisions. For more central interactions there is no such leading fragment, and these interactions may be related to the multifragmentation processes.

The above presented features of the Pb projectile fragmentation clearly show a variety of the observed fragmentation modes. This can be further illustrated by studying the relation between $(Q_f - Z_1)$ and Z_1, where $Q_f = \sum Z_f + 2N_\alpha + N_s(\eta \geq 6.26)$. The Q_f therefore denotes the sum of charges of all particles (including those with charge $Z = 1$) emitted within the fragmentation cone of the projectile nucleus (see Section 2 for explanation of the η value used to define the projectile fragmentation region). The relation between $(Q_f - Z_1)$ vs Z_1 is shown in Fig.12. A solid line in Fig.12 corresponds to Q_f equal to the projectile charge (Z_p). A significant fraction of the events is distributed along this straight line, which indicates that in these events the charge confined within a cone $\eta \geq 6.26$ equals the charge of the Pb projectile. confined within a cone $\eta \geq 6.26$ equals the charge of the Pb projectile. The spread of points around this line is partially due to the uncertainties in charge measurements. Additionally, points situated above the line may correspond to the events in which produced particles populate also the fragmentation region, whereas those below the line may correspond to the events in which some of projectile protons interacted with

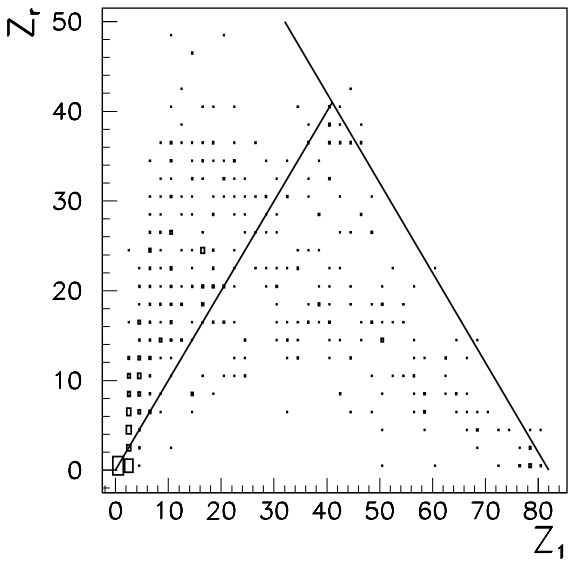

Fig. 10. Correlation between charge of the heaviest fragment, Z_1, and remaining bound charge, Z_r. Left diagonal line correspond to $Z_r = Z_1$, and the right one shows charge limit.

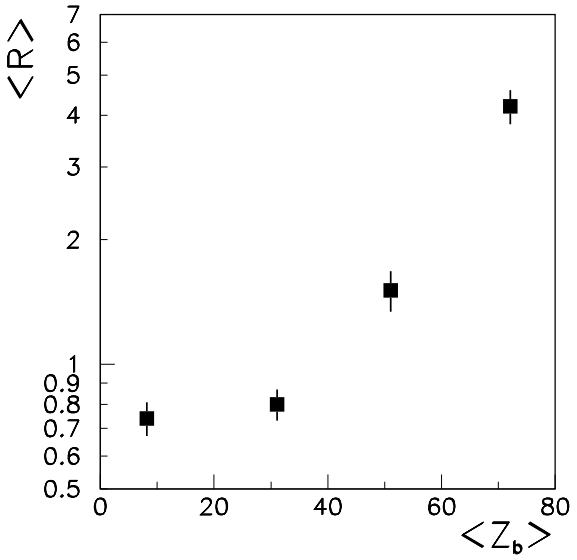

Fig. 11. Average value of the ratio R (see the text for R definition) as a function of the average bound charge.

the target nucleons and were scattered at larger angles. In Fig. 12 we can also observe a group of events characterized by small values of both Z_1 and Q_f. These are due to central Pb–Pb collisions, in which many nucleon–nucleon interactions took place, leading to a violent disruption of the projectile.

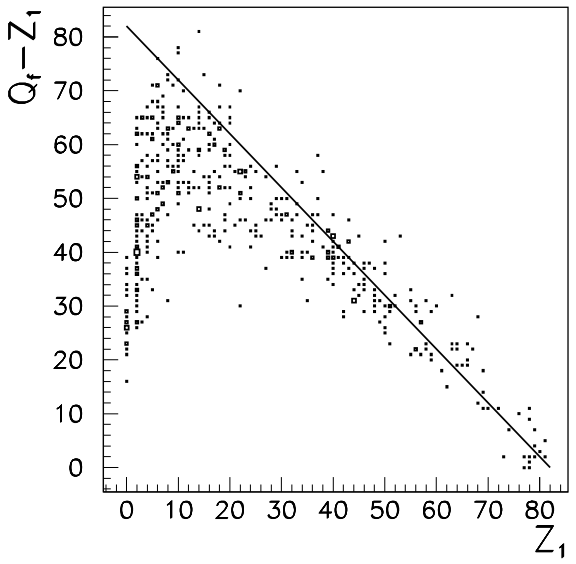

Fig. 12. Correlation between $(Q_f - Z_1)$ and Z_1. The line corresponds to $Q_f = Z_p$.

4.2. Fission

Among various fragmentation channels, there is a well defined class of events corresponding to the fission of the Pb nucleus. These are characterized by the emission of two heavy fragments carrying together practically all of the projectile charge. The evidence for such events could be already seen in Fig. 7. We have selected 18 fission-like events satisfying the following criteria: $N_f = 2$, $Z_1 \geq Z_2 \geq 20$ and $\Delta Z = Z_p - (Z_1 + Z_2) \leq 5$. It should be pointed out that our scanning procedure is 100 % efficient for finding this type of events. The average characteristics of these events are listed in Table I. The charges of the fission products indicate that the observed fission of the Pb nucleus is a symmetric process. Namely the asymmetry parameter, $S = (Z_1 - Z_2)/(Z_1 + Z_2)$ is very small and equals 0.09 ± 0.02. The observed fission events correspond to the cross section of $\sim$ 340 mb, which exceeds the cross section of 142 ± 14 mb measured for fission of Pb target nucleus bombarded by 1 GeV protons [20]. Thus, we see an increase of the cross section for fission of the Pb nucleus between the energy of 1 to 158 GeV/nucleon. This observation can be explained by the following

argument: the threshold energy for fission of Pb nuclei is low, of the order of 35 MeV, and majority of fission events observed at high energy can be induced by electromagnetic processes, while at lower energies (of the order of 1 GeV/nucleon) the processes of electromagnetic fission are suppressed (see the discussion in the previous Section). This observed increase of the cross section for fission of Pb nuclei is in contrast to the reported [3] decrease of the cross section for fission of gold nuclei from 1 to 10.6 GeV/nucleon. However, the Pb nucleus which has a magic number of neutrons and protons, might be expected to show different fission behavior.

4.3. Multifragmentation

Another type of fragmentation process, recorded efficiently in our experiment, is the multifragmentation in which a heavy projectile breaks-up into many fragments of relatively small charges. In the last several years the study of multifragmentation of heavy ions has attracted a lot of interest caused by the possible relation of this process to a liquid-gas phase transition [21]. Despite numerous experimental investigations of this process, the question whether multifragmentation can be associated with a phase change or is a purely statistical process, remains open. There is no commonly accepted definition of multifragmentation processes. In our approach, we have selected events with at least three light N_f fragments as representative for multifragmentation. By the light fragment we assume a fragment with a charge $Z_f \leq 15$. Such fragments are most frequent as it is shown in Fig. 7. 67 events fulfill the above requirements and their average properties are quoted in the last column of Table I. The charge distribution for multifragmentation can be described by exponential dependence $P(Z_f) \sim \exp^{-\mu Z_f}$, (see Fig. 13), with the coefficient $\mu = 0.23 \pm 0.02$ and χ^2 of 0.88 per degree of freedom. Fig. 14 shows the fragment multiplicity distribution. Within statistical error bars this distribution is consistent with the Poisson distribution. The correlations between the azimuthal emission angles (angles in the plane perpendicular to the Pb beam) of fragments were also studied. In Fig. 15 the distribution of relative angles between fragments is displayed. This distribution is approximately constant suggesting an isotropic emission of fragments in multifragmentation events. The Poissonian multiplicity distribution and the lack of angular correlations confirms the random character of fragment evaporation. These two observations, therefore, favor the statistical interpretation of multifragmentation processes.

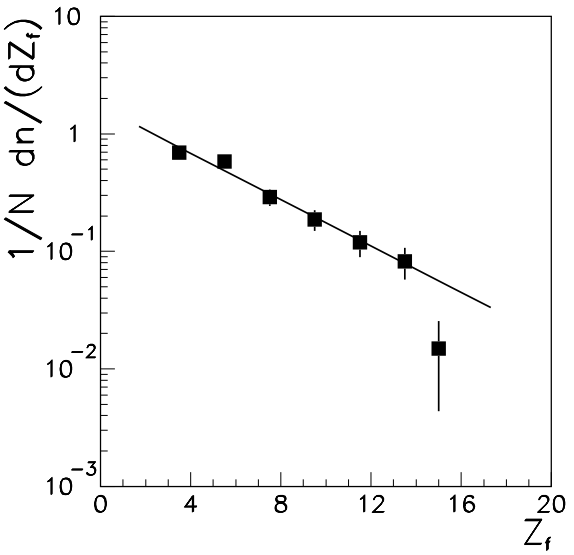

Fig. 13. The charge distribution of fragments for multifragmentation events. The line is an exponential fit to the data points.

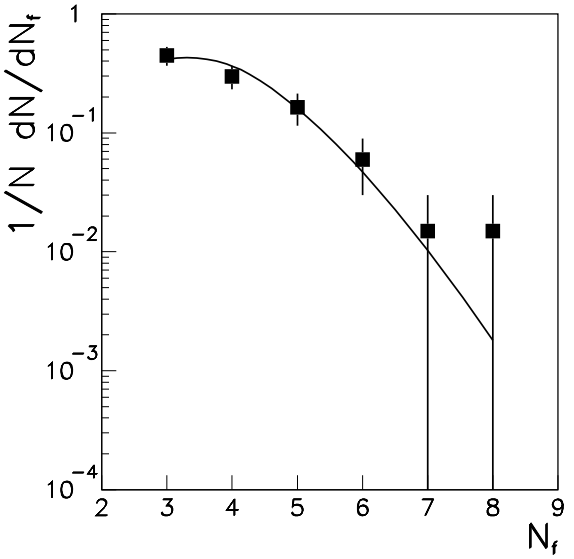

Fig. 14. Multiplicity distribution of N_f fragments in multifragmentation events with the Poisson fit.

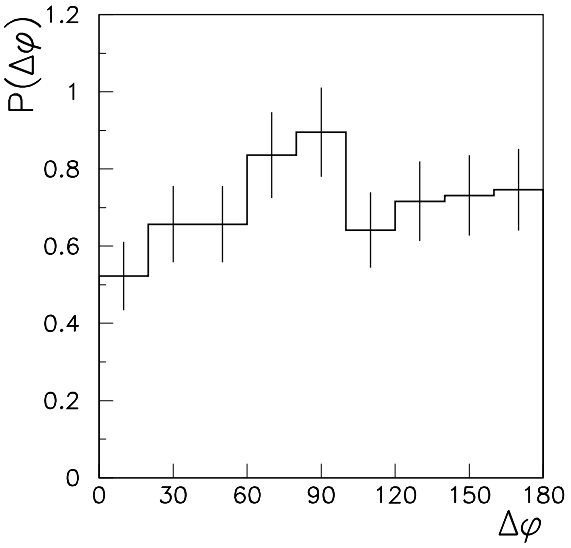

Fig. 15. Distribution of relative azimuthal angles between fragments emitted in multifragmentation processes.

5. Summary and conclusions

The lead-emulsion chambers composed of the target, angular measurement and charge identification modules appear to be a suitable tool for the analysis of high energy (158 GeV/nucleon) Pb projectile fragmentation processes. It has been found that the experimentally determined cross section of Pb–Pb interactions is greater than the predicted nuclear charge changing cross section. The only reasonable explanation was an increased contribution of electromagnetic processes to the Pb projectile fragmentation. The observed events of Pb–Pb fragmentation caused by electromagnetic dissociation do not differ significantly from the break-up caused by nuclear processes and therefore the presented results refer to a sample of events being a mixture of about 80 % of nuclear origin and the rest of electromagnetic nature.

Helium fragments are the most frequent among the multiply charged projectile fragments. The multiplicity distribution of helium fragments is flat up to 7 and extends up to 14. It should be stressed that alpha particles are present whenever there are more than two heavier fragments emitted. The multiplicity distribution of fragments heavier than alpha particles has a maximum at 1–2 and extends only up to 8. The charge distribution of fragments is strongly peaked for light fragments and has a tail which extends up to the charge of the Pb projectile. The lack of any increase in the vicinity of the charge of the projectile suggests that the properties of the fraction of the recorded electromagnetic events present in our sample of Pb fragmentation

are similar to the properties of the events caused by nuclear fragmentation. The same conclusion can be drawn from the distribution of the total charge bound in multiply charged projectile fragments. This distribution is flat and shows no increase for a large charge confined in multiply charged fragments.

There is a variety of fragmentation channels present in our sample. One of them is the fission of the Pb nucleus into two fragments similar in charge. We observe an increase of the cross section for fission of the Pb nucleus with the increasing energy from 1 to 158 GeV/nucleon. The other fragmentation channel is the multifragmentation process in which heavy projectile breaks up into many fragments. The multiplicity distribution of these fragments is Poisson like and they do not show any angular correlations. These observations support the hypothesis of the statistical nature of multifragmentation processes.

This work was partially supported in Poland by the State Committee for Scientific Research Grant 2P03B18409 and MSC Fund II PAA/NSF-96-256, in the U.S. by the National Science Foundation (Grant PHY-513997 at LSU) and Department of Energy (DOE-FG02-89ER40528 at Minnesota).

REFERENCES

[1] A. Dąbrowska *et al., Phys. Rev.* **D47**, 1751 (1993); *Phys. Rev.* **C40**, 66 (1989).

[2] M.I. Adamovich *et al., Phys. Rev. Lett.* **62**, 2801 (1989); G. Singh, K. Sengupta, P.L. Jain, *Phys. Rev.* **C42**, 1757 (1990); *Phys. Rev.* **C41**, 999 (1990); G. Baroni *et al.*, *Nucl. Phys.***A531**, 691 (1991); *Nucl. Phys.* **A516**, 673 (1990).

[3] C.J. Waddington, *Int. J. Mod. Phys.* **E2**, 739 (1993); R. Holynski, *Nucl. Phys.* **A566**, 191c (1994); M.L. Cherry *et al., Z. Phys.* **C62**, 25 (1994).

[4] M.L. Cherry *et al., Phys. Rev.* **C52**, 2652 (1995).

[5] M.L. Cherry *et al., Z. Phys.* **C63**, 549 (1994).

[6] M.L. Cherry *et al., Z. Phys.* **C73**, 449 (1997).

[7] M.L. Cherry *et al.*, accepted for publication in *Europ. Phys. J.*

[8] P.L. Jain, G. Singh, M.S. El-Nagdy, *Phys. Rev. Lett.* **68**, 1656 (1992); M.I. Adamovich *et al., Phys. Lett.* **B338**, 397 (1994); M.I. Adamovich *et al., Z. Phys.* **A359**, 277 (1997); P.L. Jain, G. Singh, A. Mukhopadhyay, *Phys. Rev.* **C50**, 1085 (1994).

[9] P. Deines-Jones *et al., Phys. Rev.* **C53**, 3044 (1996).

[10] W. Wolter *et al.*, 25th Int. Cosmic Ray Conf., Durban, South Africa, 1997, Vol.6, p.5

[11] B.S. Nilsen *et al., Phys. Rev.* **C52**, 3277 (1995).

[12] K. Werner, Preprint HD-TVP-93-91, (1993).

[13] C.A. Bertulani, G. Baur, *Phys. Rep.* **163**, 299 (1988).

[14] C.F. Weizsäcker, *Z. Phys.* **88**, 612 (1934); E.J. Williams, *Phys. Rev.* **45**, 729 (1934); J.D. Jackson, *Classical Electrodynamics*, Wiley, NY 1975.

[15] C.A. Bertulani, G. Baur, *Nucl. Phys.* **A442**, 739 (1985).

[16] J.W. Norbury, M.L. Waldsmith, *Phys. Rev.* **C57**, 1525 (1998).

[17] S. Datz *et al.*, *Phys. Rev. Lett.* **79**, 3355 (1997).

[18] C. Brechtmann, W. Heinrich, *Z. Phys.* **A330**, 407 (1988); *Z. Phys.* **A331**, 463 (1988).

[19] C. Chollet *et al., Phys. Lett.* **127B**, 331 (1983); Particle Data Group, *Phys. Lett.* **B204**, 1 (1988).

[20] L.A. Vaishnene *et al., Z. Phys.* **A302**, 143 (1981).

[21] L.P. Csernai, J.I. Kapusta, *Phys. Rep.* **131**, 223 (1986); L.G. Moretto, G.J. Wozniak, *Ann. Rev. Nucl. Part. Sci.* **43**, 374 (1993).